Journal of Materials Chemistry C

ROYAL SOCIETY OF CHEMISTRY

PAPER

View Article Online
View Journal | View Issue

Cite this: J. Mater. Chem. C, 2023, 11, 3581

Accelerated polaron formation in perovskite quantum dots monitored *via* picosecond infrared spectroscopy†

Matthias Nuber, [a] Qi Ying Tan, [bc] Daniel Sandner, [a] Jun Yin, [f] Reinhard Kienberger, [a] Cesare Soci *[de] and Hristo Iglev *[a]

Received 24th October 2022,
Accepted 5th February 2023

DOI: 10.1039/d2tc04519b

rsc.li/materials-c

The formation and nature of polarons in perovskite quantum dots (QDs) are still unclear. Due to the very limited crystal size and quantum confinement, influences on the polaron stabilization dynamics could be expected. Here, we investigate the coupling of photoexcited charges to vibrational modes in mixed cation lead halide $Cs_{0.2}FA_{0.8}PbBr_3$ QDs *via* picosecond mid-infrared spectroscopy in comparison to the bulk film. We find additional processes occurring in an infrared activated vibrational (IRAV) mode compared to the ground-state bleaching and screened carrier background signal. Using that mode as a proxy for the charge-molecular bond coupling, we interpret additional time constant as a polaron stabilization time. With the confinement effects present in the QDs, this time shortens from tens of picoseconds in the bulk to only a few picoseconds.

Introduction

Constraining the dimensionality of optoelectronic materials leads to a plethora of new effects and changes in optical properties. In particular, for perovskites, the reduction of the sample dimension, be it to 2D layers in the form of Ruddlesden–Popper systems or as a nanoparticle restricting the overall size of the crystal, has been employed for many applications.[1,2] Perovskite nanocrystals show a high defect tolerance[3] in their bright luminescence[4,5] and have demonstrated high power conversion efficiencies in solar cells.[6,7] Although the adaptability of the electronic properties of the perovskite material might be the most prominent effect of the reduction in dimension, it also affects the susceptibility to degradation processes induced by water or oxygen.[8]

Focusing on perovskite nanocrystals, one can distinguish between larger nanocrystals (NCs), in which the electronic properties of the perovskite material are relatively unperturbed, and quantum dots (QDs), in which quantum confinement effects play a relevant role.[9] In the latter, emission and absorption features of the perovskite generally blue-shift with decreasing system size.[10] A particular popular perovskite quantum dot system is $CsPbBr_3$, together with its organic homologues such as the formamidinium-based $FAPbBr_3$. For both systems, a high stability and a widely tunable band gap, and thereby emission energy have been reported.[11,12] For most applications in which QDs are envisioned, the charge carrier dynamics and interactions after photoexcitation are of high relevance. A first key aspect when discussing the dynamics of charge carriers concerns the initial charge carrier density, in this case in the form of the average number of charges within one NC. If this value is well below one, no non-geminate processes are possible and therefore recombination on the nanosecond time-scale dominates.[13] Exceeding this value, as in the experiments discussed here, leads to the interaction of multiple charge carriers confined within the NC.

The dynamics and nature of the photoexcited charge carriers in $CsPbBr_3$ and $FAPbBr_3$ QDs and NCs have been explored in the literature. Li *et al.*[14] described how the bimolecular recombination rate in confined QDs is size-dependent with the decay times rising as the QD size increases. They reported this effect

[a] Lehrstuhl für Laser- und Röntgenphysik, Physik-Department, TUM School of Natural Sciences, Technische Universität München, James-Franck-Str. 1, 85748 Garching, Germany. E-mail: higlev@ph.tum.de
[b] Centre for Disruptive Photonic Technologies, The Photonics Institute, Nanyang Technological University, 21 Nanyang Link, 637371, Singapore
[c] Interdisciplinary Graduate School, Energy Research Institute @NTU (ERI@N), Nanyang Technological University, 50 Nanyang Drive, 637553, Singapore
[d] Centre for Disruptive Photonic Technologies, The Photonics Institute, Nanyang Technological University, 21 Nanyang Link, 637371, Singapore
[e] Division of Physics and Applied Physics, School of Physical and Mathematical Sciences, Nanyang Technological University, 21 Nanyang Link, 637371, Singapore. E-mail: csoci@ntu.edu.sg
[f] Department of Applied Physics, The Hong Kong Polytechnic University, Kowloon 999077, Hong Kong, P. R. China

† Electronic supplementary information (ESI) available: Experimental methods; sample preparation; DFT-spectra and methods; and additional TCSPC data showing bimolecular effects on ns time scales. See DOI: https://doi.org/10.1039/d2tc04519b

to be very similar for the inorganic cesium cation and the organic formamidinium cation. Although polaron formation is generally considered to be a key factor in three-dimensional perovskites, for quantum confined systems, a different charge–lattice interaction could be imagined. In some publications,[13,14] the charge carriers are, indeed, described to be of excitonic nature. Nevertheless, Kaur *et al.* demonstrated in their articles,[15–17] using visible transient absorption spectroscopy, how polarons form in NCs within the first picosecond and argue that their size considerably exceeds the lattice parameter of the perovskite crystal. In similar experiments, Sonnichsen *et al.*[18] reported a smaller polaron size and described them as quantum confined exciton polarons. With time-resolved X-ray absorption spectroscopy, more focused on the structural effect of polaron formation, Cannelli *et al.*[19] monitored the structural polaron signal in 10 nm QDs.

Albeit the literature already offers insight into the general polaron properties of perovskite QDs, a comprehensive understanding of the specific interaction of the photoexcited charge carriers and the crystal structure is still lacking. In particular, a deeper knowledge of the coupling of polarons to vibrational bonds and the influence of the restricted size in the quantum-confined QDs might offer new paths for sample optimization and application in combination with other emerging materials.

In this article, we investigate the coupling of polarons to an organic CN mode of the formamidinium cation in mixed cation lead halide $Cs_{0.2}FA_{0.8}PbBr_3$ perovskite QDs in comparison with the bulk film by mIR transient absorption spectroscopy. Thereby, we are particularly sensitive to polaron formation and screening processes.[20] We observe a broad transient electronic polaron absorption overlayed by a transient ground-state bleaching and infrared activated mode signal at the vibrational mode of the organic cation. From an analysis of the dynamics of these characteristic signals, we find that the vibration-related signal has a different dynamic than the excited population associated background at early delay times. We associate that difference with the occurrence of a polaron screening process. The confinement in the QDs leads to a shortening of that additional process, indicating a faster polaron formation time. Our findings add to the ongoing debate on the polaron properties in perovskite NCs and QDs.

Results and discussion

Perovskite nanocrystals and quantum dots are often produced by the ligand-assisted reprecipitation method.[21] Here, we used oleylamine and oleic acid to form quantum dots in a DMF solution. The bulk film samples were produced by spin-coating (more details for both samples, and for the experimental methods in general, can be found in the ESI†). As the size and size distribution of perovskite nanocrystals strongly depends on the fabrication method,[22] a thorough characterization is required. In addition to spectroscopic analysis that will be discussed below, transmission electron microscopy (TEM) allows imaging of the quantum dots fabricated and thereby directly measuring their size, shape and size distribution. In

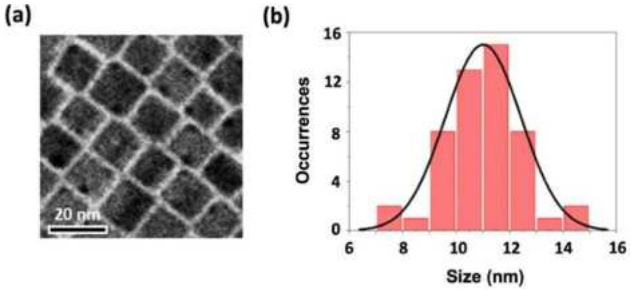

Fig. 1 (a) TEM image of the $Cs_{0.2}FA_{0.8}PbBr_3$ perovskite QDs. Size distribution of $Cs_{0.2}FA_{0.8}PbBr_3$ perovskite QDs as determined from TEM analysis.

Fig. 1a, part of a TEM image is depicted with the distribution of nanocrystal sizes shown in Fig. 1b. We find that the rectangular NCs have a size of (11 ± 1) nm.

Apart from the reduction in the crystal size, leading to a limited space for diffusion, crystals with size small enough to induce quantum confinement effects experience changes in their electronic properties reflected by the absorption and photoluminescence (PL) spectrum. Thereby, a distinction between nanocrystals in general and quantum dots can be made from spectroscopy.

In Fig. 2a and b, the absorbance and PL signal of the $Cs_{0.2}FA_{0.8}PbBr_3$ perovskite QDs and the $Cs_{0.2}FA_{0.8}PbBr_3$ bulk film are shown. One can clearly see that both, the symmetric PL spectra as well as the absorbance signal with a characteristic band-gap onset, are blue-shifted upon quantum confinement. From the PL spectra, this effect can be quantified to approximately 40 meV. We can therefore conclude that the 11 nm-size nanocrystals employed here can be considered as quantum dots and are subject to quantum confinement effects which can also be seen in their single photon emission characteristics published elsewhere.[23]

As we are using time-resolved vibrational spectroscopy to examine the excited perovskite samples, an infrared ground-state characterization of the samples is required. In Fig. 2c, FTIR spectra of the QDs and the bulk film can be seen. Due to the restricted probe range of the transient set-up, but also of

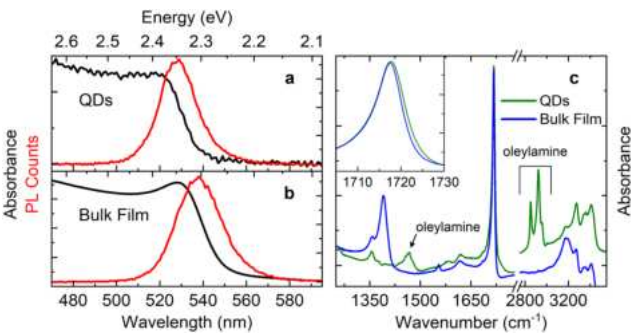

Fig. 2 (a) and (b): Normalized absorbance (in black) and photoluminescence (in red) spectra of $Cs_{0.2}FA_{0.8}PbBr_3$ perovskite QDs (a) and $Cs_{0.2}FA_{0.8}PbBr_3$ bulk film (b). (c) Normalized FTIR spectra of both samples with the inset showing the vibrational mode at 1717 cm^{-1} in more detail. For the QDs, modes originating from oleylamine ligand are indicated.

standard FTIR devices, employed, only vibrational modes of organic components, in this case the organic formamidinium cation, can be monitored. Vibrational modes of the inorganic parts of the perovskite crystal would be expected at considerably lower energies.[24,25] The spectra are dominated by a single comparatively sharp and isolated mode at 1717 cm^{-1}. From the DFT-calculations performed (more on the computational methods employed can be found in the ESI,† including the spectrum in Fig. S1, ESI† and the visualized modes in Fig. S2, ESI†) as well as from the literature,[24,26,27] we can assign this mode to a C═N stretching mode. In the transient spectra below, we employ this mode as an indicator for the vibrational reaction of the perovskite crystal after charge carrier generation and polaron formation. A series of FTIR-measurements over a wide temperature range shows that there is only a very limited blue-shift upon heating the samples (see the ESI† for more details including Fig. S3). In addition to the dominating mode at 1717 cm^{-1}, vibrational signals can be found as NH_2 modes at lower frequencies (a detailed discussion and mode assignment can be found in the ESI†). Although most spectral features are very similar for the bulk film and the QDs, we find that the mode around 1390 cm^{-1} is suppressed for the quantum confined crystal. Comparing with the spectra from the literature,[26,28] albeit not explicitly mentioned there, this effect appears to be a reproducible feature. As our focus in this article is on time-resolved spectra in proximity of another vibrational mode, a detailed analysis of this effect is beyond the scope of our work here.

To obtain transient spectra and investigate their dynamics, we excited both samples with ultrashort pulses of 525 nm. A delayed mid-infrared (mIR) probe pulse then resolves transient changes in the mIR absorption of the samples. The best time-resolution is on the order of 0.5 ps with a maximum time delay of 2 ns (more details on the experimental set-up can be found in the ESI†). In general, two features can be expected in transient mIR spectra. Firstly, electronic absorption of screened carriers, often described as polarons, lead to very broad and unstructured transient absorption features.[29] These signals can be used as a proxy for the overall polaron population. Secondly, specific vibrational signals, originating from the molecular bonds of the material investigated, offer insight into structural rearrangements upon photoexcitation. These vibrational signals can occur in a plethora of forms, including the bleaching of the ground-state, red- or blue-shifts of a mode or the rise of an infrared activated vibration and excited state vibrations. They can elucidate the charge distribution processes in the excited state[30] as well as polaron formation and evolution.[20,31] In Fig. 3, transient infrared spectra are shown for selected delay times. As described above, both a broad background as well as a specific vibrational response can be observed for both samples investigated. At early delay times, the vibrational signal resembles a ground state mode blue-shifting with its characteristic "valley-peak" signature. At later delay times though, the negative absorbance change signal vanishes earlier than the excited state absorption (see Fig. 3d and e for normalized background-subtracted spectra) which we associate with an infrared activated vibration (IRAV) mode. The IRAV mode is split for the bulk film sample, a feature that is not present in the QDs. A comparison with temperature-resolved FTIR spectra (see Fig. S3 in the ESI†) ensures that a temperature-induced shift in the vibrational frequency is not plausible.

To discuss the different signals in more detail, in Fig. 4, the dynamics of the background-subtracted IRAV mode, the background-subtracted bleaching signal and the background signal at one of the edge pixels of the detector are depicted with suitable *y*-axes and for different excitation densities. We can

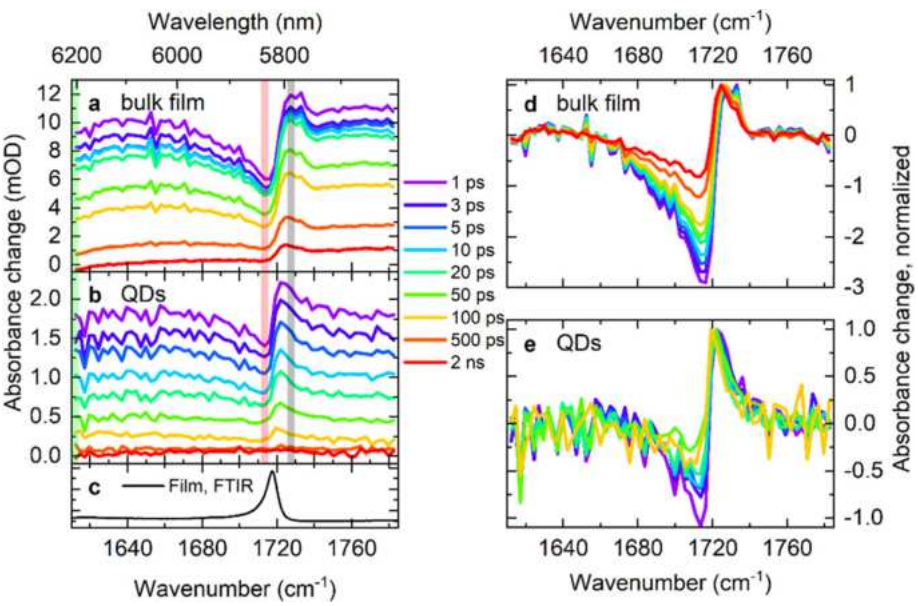

Fig. 3 (a and b) Transient spectra of the $Cs_{0.2}FA_{0.8}PbBr_3$ bulk film and QDs at selected delay times. (c) FTIR spectrum as a reference. (d and e) Normalized (to the peak of the IRAV mode) background-subtracted spectra of $Cs_{0.2}FA_{0.8}PbBr_3$ bulk film and QDs.

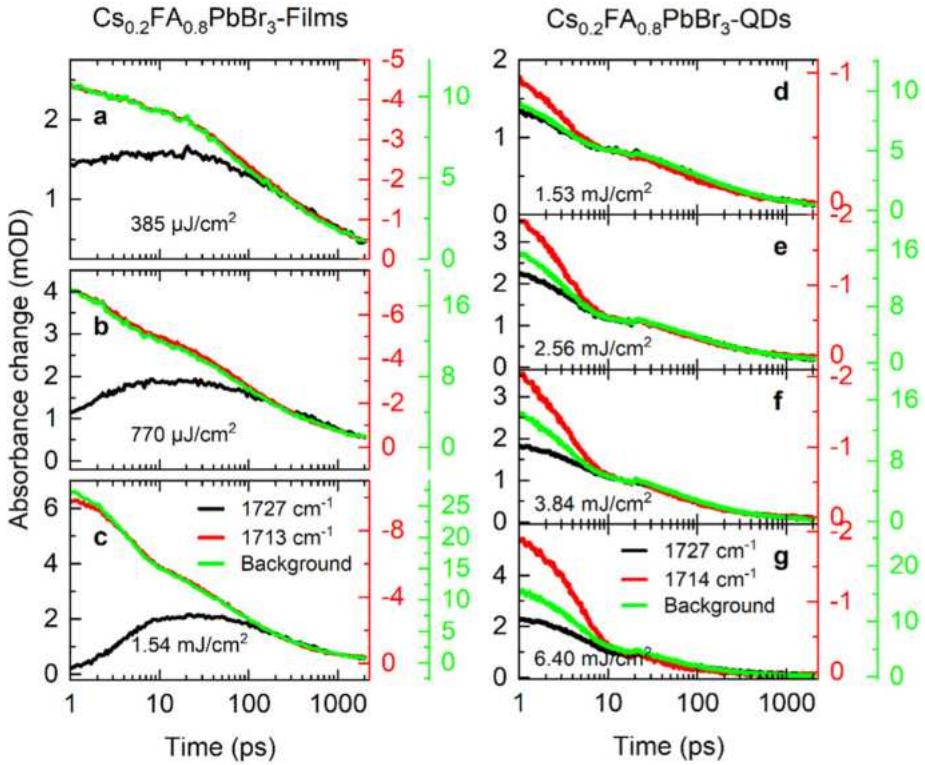

Fig. 4 Dynamics of characteristic spectral features in $Cs_{0.2}FA_{0.8}PbBr_3$ perovskite bulk films (a–c) and $Cs_{0.2}FA_{0.8}PbBr_3$ QDs (d–f) with different excitation densities. The signal at 1727 cm^{-1} refers to the IRAV mode, the signal at 1713/1714 cm^{-1} to the ground-state bleaching and the background dynamics is evaluated at 1612 cm^{-1}.

clearly see that for the bulk film sample, the background signal and the ground-state bleaching signal share exactly the same dynamics while the IRAV mode increases in intensity for the first few picoseconds and has a different dynamic for the first hundred picoseconds. We find that although the background and bleaching signal exhibit some excitation-density dependence that originates from multiple carrier interactions (see also time-resolved PL measurements in the ESI†), the time from which IRAV mode and the other spectral components share the same recombination dynamics appears to be independent of the initial charge-carrier density, implying a monomolecular process. Looking at the QDs, two key differences in the dynamics can be observed. Firstly, the point in time from which on the different spectral features share the same dynamics is far earlier, at a few picoseconds. Secondly, at these early delay times, all three features, the polaronic background, the ground-state bleaching signal and the IRAV mode experience different signal dynamics. In particular, the vibrational ground-state bleaching shows the strongest relative early decay, followed by the background signal and the IRAV mode. Considering the ground-state bleaching signal as a proxy for a large variety of possible photoexcitations, be it excitons or screened polaronic carriers, and the electronic background signal as an indicator for polarons, the difference in weight for the earliest few ps process points towards a relevant portion of charge carriers that are not screened in QDs and have a very fast decay mechanism. In the literature, polaron formation in perovskites is generally considered to be advantageous for the carrier lifetimes.[32]

For a more detailed discussion of our main finding, the vast difference dynamics between the IRAV mode and the ground-state bleaching or background signal, a closer look at the interactions leading to IRAV modes is required. In the literature, these modes have been associated with polarons in both organic semiconductors[30,33] as well as in perovskites.[34,35] Albeit there is no definite explanation for IRAV modes yet and the term might be used as an umbrella term for different physical interactions, they are regularly associated with a change in the vibrational bond they are based upon. A first concept views IRAV modes to be a result of an activation of Raman-modes that are not present in the molecules ground-state IR spectrum but that become so due to a charge redistribution in the excited state.[36] In a second concept, IRAV modes are ascribed to the very similar energy between an electronic transition and a vibrational mode, as well as a strong coupling of the charge redistribution to nuclear motion.[37] That is reflected in an enhancement of IR mode intensity. For both approaches, a strong interaction between the photoinduced structural changes that accompany a polaron formation and the IRAV mode strength can be concluded. Therefore, the IRAV mode signal can be used as an indicator to monitor the polaron formation and development in our samples. In very similar systems, excited state absorptions akin to the signal described here have been reported in the literature. Taylor *et al.*[34] reported a transient infrared mode of the

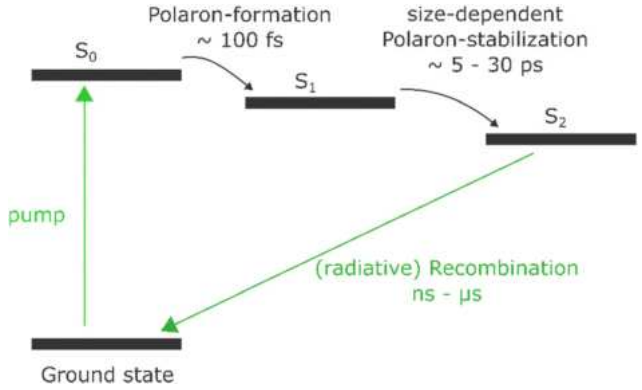

Fig. 5 This scheme shows the charge carrier dynamics that we associate with the observed pump–probe transients. The material is excited by the pump pulse and the excited state undergoes several transitions by structural arrangements of the lattice. Recombination returns the system to its ground state.

same C–N vibration blue-shifted to the ground-state mode in $FAPbI_3$ and associated that signal with an IRAV mode due to an enhanced vibrational transition dipole moment. Guo *et al.*[38] also reported similar effects after photoexcitation. In a recent study, Nishida *et al.*[39] also described a blue-shifted transient vibrational response overlaying a broad polaronic background.

Considering the close relation between the IRAV mode and the formation of polarons in a sample, as discussed above, the additional dynamics at early delay times can be interpreted as a time constant in the polaron evolution. With the first screening process occurring within our temporal resolution of approximately 0.5 ps, as indicated by the immediate rise of the screened carrier background signal, the interactions present in our measurements can be conceptualized with a stabilization and consolidation of the polaron. The time scales we observe here, a few ps for the QDs and few tens of ps for bulk films, coincide with structural rearrangement processes due to polaron formation proposed in the literature.[20,40] As at later delay times, the IRAV mode, and thereby the interaction strength of the polaron and the CN vibrational mode, share the same dynamics as the overall screened carrier population and the ground-state bleaching the coupling of the photoexcited charge carriers can be assumed to be concluded. Later effects can thus be related to charge recombination processes that both lead to a vanishing polaron signal in the background and the IRAV mode as well as a filling-up of the ground state. With the QDs showing a considerably faster polaron stabilization process than the bulk films with an ''infinite'' lattice, we can reason that confinement effects influence the coupling of a polaron and a vibrational mode relevantly. Apparently, in perovskite QDs, that process is finished approximately an order of magnitude faster than in the bulk film of the same material.

Fig. 5 summarizes our proposed model for polaron formation and stabilization. Immediately after excitation we observe a spectrally broad signal that can be associated with free carriers or polarons (state S_1). Limited by the temporal resolution in our experiments we cannot make further statements about the nature of S_0, which is most likely an excitonic state. Because of the sensitivity of the IRAV mode at 1727 cm^{-1} we can track the structural re-arrangement induced by the photoexcited charge carriers. This transition to a strongly localized carrier (state S_2) is size dependent with approximate time constants of 5 and 30 ps for $Cs_{0.2}FA_{0.8}PbBr_3$ QDs and bulk films, respectively. Over the span of hundreds of ps, nanoseconds and microseconds we find radiative recombination by which the system returns to its ground state. Since this process requires two carriers, an electron and a hole, the recombination rate and lifetime are highly carrier density dependent. In contrast, the polaron stabilization time in our experiments was found to be constant under a magnitude of excitation intensities and is therefore linked to carrier-lattice coupling.

Conclusions

Using transient mIR spectroscopy, we exploit the difference in signal dynamics between a blue-shifted polaron-associated IRAV mode at an organic cationic vibration, the ground-state bleaching signal of that mode and a wide electronic background associated with screened carriers. Thereby, we find polaron formation processes reflected in an additional early delay mechanism which we associate with polaron evolution and stabilization. That process is around an order of magnitude faster in $Cs_{0.2}FA_{0.8}PbBr_3$ perovskite QDs than in $Cs_{0.2}FA_{0.8}PbBr_3$ bulk films. Our findings broaden the knowledge of the specific polaron properties in confined perovskite nanocrystals and might provide new directions for further experiments on the structural dynamics and conductivity effects of polaron formation in nanocrystals.

Conflicts of interest

The authors declare no competing interest.

Acknowledgements

This research was supported by the Deutsche Forschungsgemeinschaft (DFG) *via* the Clusters of Excellence ''e-conversion'' EXC 2089/1-390776260 and ''Munich Center for Quantum Science and Technology (MCQST)'' EXC 2111/390814868, and by the Singapore Agency for Science, Technology and Research A*STAR-AME programmatic grant on Nanoantenna Spatial Light Modulators for Next-Gen Display Technologies (Grant no. A18A7b0058). M. N. thanks the ''Studienstiftung des deutschen Volkes'' for a PhD scholarship.

References

1 D. Chen and X. Chen, Luminescent perovskite quantum dots: synthesis, microstructures, optical properties and applications, *J. Mater. Chem. C*, 2019, 7(6), 1413–1446, DOI: 10.1039/C8TC05545A.

2 H. Chen, J. M. Pina, Y. Hou and E. H. Sargent, Synthesis, Applications, and Prospects of Quantum-Dot-in-Perovskite

Solids, *Adv. Energy Mater.*, 2022, **12**(4), 2100774, DOI: 10.1002/aenm.202100774.

3 H. Huang, M. I. Bodnarchuk, S. V. Kershaw, M. V. Kovalenko and A. L. Rogach, Lead Halide Perovskite Nanocrystals in the Research Spotlight: Stability and Defect Tolerance, *ACS Energy Lett.*, 2017, **2**(9), 2071–2083, DOI: 10.1021/acsenergylett.7b00547.

4 Y. Kim, E. Yassitepe, O. Voznyy, R. Comin, G. Walters, X. Gong, P. Kanjanaboos, A. F. Nogueira and E. H. Sargent, Efficient Luminescence from Perovskite Quantum Dot Solids, *ACS Appl. Mater. Interfaces*, 2015, **7**(45), 25007–25013, DOI: 10.1021/acsami.5b09084.

5 F. Liu, Y. Zhang, C. Ding, S. Kobayashi, T. Izuishi, N. Nakazawa, T. Toyoda, T. Ohta, S. Hayase, T. Minemoto, K. Yoshino, S. Dai and Q. Shen, Highly Luminescent Phase-Stable CsPbI3 Perovskite Quantum Dots Achieving Near 100% Absolute Photoluminescence Quantum Yield, *ACS nano*, 2017, **11**(10), 10373–10383, DOI: 10.1021/acsnano.7b05442.

6 J. Yuan, A. Hazarika, Q. Zhao, X. Ling, T. Moot, W. Ma and J. M. Luther, Metal Halide Perovskites in Quantum Dot Solar Cells: Progress and Prospects, *Joule*, 2020, **4**(6), 1160–1185, DOI: 10.1016/j.joule.2020.04.006.

7 F. Li, S. Zhou, J. Yuan, C. Qin, Y. Yang, J. Shi, X. Ling, Y. Li and W. Ma, Perovskite Quantum Dot Solar Cells with 15.6% Efficiency and Improved Stability Enabled by an α-CsPbI 3/FAPbI 3 Bilayer Structure, *ACS Energy Lett.*, 2019, **4**(11), 2571–2578, DOI: 10.1021/acsenergylett.9b01920.

8 C. G. Sanjayan, M. S. Jyothi and R. G. Balakrishna, Stabilization of CsPbBr 3 quantum dots for photocatalysis, imaging and optical sensing in water and biological medium: a review, *J. Mater. Chem. C*, 2022, **10**(18), 6935–6956, DOI: 10.1039/D2TC00340F.

9 P. Kambhampati, Nanoparticles, Nanocrystals, and Quantum Dots: What are the Implications of Size in Colloidal Nanoscale Materials?, *J. Phys. Chem. Lett.*, 2021, **12**(20), 4769–4779, DOI: 10.1021/acs.jpclett.1c00754.

10 L. Protesescu, S. Yakunin, M. I. Bodnarchuk, F. Krieg, R. Caputo, C. H. Hendon, R. X. Yang, A. Walsh and M. V. Kovalenko, Nanocrystals of Cesium Lead Halide Perovskites ($CsPbX_3$, X = Cl, Br, and I): Novel Optoelectronic Materials Showing Bright Emission with Wide Color Gamut, *Nano Lett.*, 2015, **15**(6), 3692–3696, DOI: 10.1021/nl5048779.

11 L. Protesescu, S. Yakunin, M. I. Bodnarchuk, F. Bertolotti, N. Masciocchi, A. Guagliardi and M. V. Kovalenko, Monodisperse Formamidinium Lead Bromide Nanocrystals with Bright and Stable Green Photoluminescence, *J. Am. Chem. Soc.*, 2016, **138**(43), 14202–14205, DOI: 10.1021/jacs.6b08900.

12 X. Zhang, H. Liu, W. Wang, J. Zhang, B. Xu, K. L. Karen, Y. Zheng, S. Liu, S. Chen, K. Wang and X. W. Sun, Hybrid Perovskite Light-Emitting Diodes Based on Perovskite Nanocrystals with Organic-Inorganic Mixed Cations, *Adv. Mater.*, 2017, **29**(18), 1606405, DOI: 10.1002/adma.201606405.

13 N. S. Makarov, S. Guo, O. Isaienko, W. Liu, I. Robel and V. I. Klimov, Spectral and Dynamical Properties of Single Excitons, Biexcitons, and Trions in Cesium-Lead-Halide Perovskite Quantum Dots, *Nano Lett.*, 2016, **16**(4), 2349–2362, DOI: 10.1021/acs.nanolett.5b05077.

14 Y. Li, T. Ding, X. Luo, Y. Tian, X. Lu and K. Wu, Synthesis and Spectroscopy of Monodispersed, Quantum-Confined FAPbBr 3 Perovskite Nanocrystals, *Chem. Mater.*, 2020, **32**(1), 549–556, DOI: 10.1021/acs.chemmater.9b04297.

15 G. Kaur, K. J. Babu and H. N. Ghosh, Temperature-Dependent Interplay of Polaron Formation and Hot Carrier Cooling Dynamics in CsPbBr3 Nanocrystals: Role of Carrier-Phonon Coupling Strength, *J. Phys. Chem. Lett.*, 2020, **11**(15), 6206–6213, DOI: 10.1021/acs.jpclett.0c01724.

16 G. Kaur and H. N. Ghosh, Hot Carrier Relaxation in CsPbBr3-Based Perovskites: A Polaron Perspective, *J. Phys. Chem. Lett.*, 2020, **11**(20), 8765–8776, DOI: 10.1021/acs.jpclett.0c02339.

17 K. Justice Babu, G. Kaur, A. Shukla, R. Saha, A. Kaur, M. Sachdeva, D. K. Yadav and H. N. Ghosh, Fast Polaron Formation and Low Carrier Mobility in Defect-Free Polyhedral CsPbBr 3 Perovskite Nanocrystals, *ACS Photonics*, 2022, **9**(3), 969–978, DOI: 10.1021/acsphotonics.1c01830.

18 C. D. Sonnichsen, D. P. Strandell, P. J. Brosseau and P. Kambhampati, Polaronic quantum confinement in bulk CsPbBr3 perovskite crystals revealed by state-resolved pump/probe spectroscopy, *Phys. Rev. Res.*, 2021, **3**(2), 023147, DOI: 10.1103/PhysRevResearch.3.023147.

19 O. Cannelli, N. Colonna, M. Puppin, T. C. Rossi, D. Kinschel, L. M. D. Leroy, J. Löffler, J. M. Budarz, A. M. March, G. Doumy, A. Al Haddad, M.-F. Tu, Y. Kumagai, D. Walko, G. Smolentsev, F. Krieg, S. C. Boehme, M. V. Kovalenko, M. Chergui and G. F. Mancini, Quantifying Photoinduced Polaronic Distortions in Inorganic Lead Halide Perovskite Nanocrystals, *J. Am. Chem. Soc.*, 2021, **143**(24), 9048–9059, DOI: 10.1021/jacs.1c02403.

20 K. Stallhofer, M. Nuber, D. Cortecchia, A. Bruno, R. Kienberger, F. Deschler, C. Soci and H. Iglev, Picosecond Charge Localization Dynamics in CH3NH3PbI3 Perovskite Probed by Infrared-Activated Vibrations, *J. Phys. Chem. Lett.*, 2021, **12**(18), 4428–4433, DOI: 10.1021/acs.jpclett.1c00935.

21 F. Haydous, J. M. Gardner and U. B. Cappel, The impact of ligands on the synthesis and application of metal halide perovskite nanocrystals, *J. Mater. Chem. A*, 2021, **9**(41), 23419–23443, DOI: 10.1039/D1TA05242J.

22 B. Chaudhary, Y. K. Kshetri, H.-S. Kim, S. W. Lee and T.-H. Kim, Current status on synthesis, properties and applications of CsPbX3(X = Cl, Br, I) perovskite quantum dots/nanocrystals, *Nanotechnology*, 2021, **32**(50), 502007, DOI: 10.1088/1361-6528/ac2537.

23 M. D'Amato, Q. Y. Tan, Q. Glorieux, A. Bramati and C. Soci, Color-Tunable Mixed-Cation Perovskite Single Photon Emitters, *ACS Photonics*, 2023, **10**(1), 197–205, DOI: 10.1021/acsphotonics.2c01437.

24 M. Mączka, J. A. Zienkiewicz and M. Ptak, Comparative Studies of Phonon Properties of Three-Dimensional Hybrid Organic–Inorganic Perovskites Comprising Methylhydrazinium, Methylammonium, and Formamidinium Cations, *J. Phys. Chem. C*, 2022, **126**(8), 4048–4056, DOI: 10.1021/acs.jpcc.1c09671.

25 P. Wang, J. Guan, D. T. K. Galeschuk, Y. Yao, C. F. He, S. Jiang, S. Zhang, Y. Liu, M. Jin, C. Jin and Y. Song,

Pressure-Induced Polymorphic, Optical, and Electronic Transitions of Formamidinium Lead Iodide Perovskite, *J. Phys. Chem. Lett.*, 2017, **8**(10), 2119–2125, DOI: **10.1021/acs.jpclett.7b00665**.

26 K. Hills-Kimball, Y. Nagaoka, C. Cao, E. Chaykovsky and O. Chen, Synthesis of formamidinium lead halide perovskite nanocrystals through solid–liquid–solid cation exchange, *J. Mater. Chem. C*, 2017, **5**(23), 5680–5684, DOI: **10.1039/C7TC00598A**.

27 R. Szostak, J. C. Silva, S.-H. Turren-Cruz, M. M. Soares, R. O. Freitas, A. Hagfeldt, H. C. N. Tolentino and A. F. Nogueira, Nanoscale mapping of chemical composition in organic-inorganic hybrid perovskite films, *Sci. Adv.*, 2019, **5**(10), eaaw6619, DOI: **10.1126/sciadv.aaw6619**.

28 H. Chen, L. Fan, R. Zhang, C. Bao, H. Zhao, W. Xiang, W. Liu, G. Niu, R. Guo, L. Zhang and L. Wang, High-Efficiency Formamidinium Lead Bromide Perovskite Nanocrystal-Based Light-Emitting Diodes Fabricated via a Surface Defect Self-Passivation Strategy, *Adv. Opt. Mater.*, 2020, **8**(6), 1901390, DOI: **10.1002/adom.201901390**.

29 M. Nuber, D. Sandner, T. Neumann, R. Kienberger, F. Deschler and H. Iglev, Bimolecular Generation of Excitonic Luminescence from Dark Photoexcitations in Ruddlesden-Popper Hybrid Metal-Halide Perovskites, *J. Phys. Chem. Lett.*, 2021, **12**(42), 10450–10456, DOI: **10.1021/acs.jpclett.1c03099**.

30 K. Stallhofer, M. Nuber, F. Schüppel, S. Thumser, H. Iglev, R. Vivie-Riedle, W. de; Zinth and H. Dube, Electronic and Geometric Characterization of TICT Formation in Hemithioindigo Photoswitches by Picosecond Infrared Spectroscopy, *J. Phys. Chem. A*, 2021, **125**(20), 4390–4400, DOI: **10.1021/acs.jpca.1c02646**.

31 K. Stallhofer, M. Nuber, R. Kienberger, V. Körstgens, P. Müller-Buschbaum and H. Iglev, Dynamics of Short-Lived Polaron Pairs and Polarons in Polythiophene Derivatives Observed via Infrared-Activated Vibrations, *J. Phys. Chem. C*, 2019, **123**(46), 28100–28105, DOI: **10.1021/acs.jpcc.9b09820**.

32 D. Meggiolaro, F. Ambrosio, E. Mosconi, A. Mahata and F. de Angelis, Polarons in Metal Halide Perovskites, *Adv. Energy Mater.*, 2019, **122**, 1902748, DOI: **10.1002/aenm.201902748**.

33 R. Österbacka, X. M. Jiang, C. P. An, B. Horovitz and Z. V. Vardeny, Photoinduced quantum interference antiresonances in pi-conjugated polymers, *Phys. Rev. Lett.*, 2002, **88**(22), 226401, DOI: **10.1103/PhysRevLett.88.226401**.

34 V. C. A. Taylor, D. Tiwari, M. Duchi, P. M. Donaldson, I. P. Clark, D. J. Fermin and T. A. A. Oliver, Investigating the Role of the Organic Cation in Formamidinium Lead Iodide Perovskite Using Ultrafast Spectroscopy, *J. Phys. Chem. Lett.*, 2018, **9**(4), 895–901, DOI: **10.1021/acs.jpclett.7b03296**.

35 W. P. D. Wong, J. Yin, B. Chaudhary, X. Y. Chin, D. Cortecchia, S.-Z. A. Lo, A. C. Grimsdale, O. F. Mohammed, G. Lanzani and C. Soci, Large Polaron Self-Trapped States in Three-Dimensional Metal-Halide Perovskites, *ACS Mater. Lett.*, 2020, **2**(1), 20–27, DOI: **10.1021/acsmaterialslett.9b00276**.

36 E. Ehrenfreund, Z. Vardeny, O. Brafman and B. Horovitz, Amplitude and phase modes in trans-polyacetylene: Resonant Raman scattering and induced infrared activity, *Phys. Rev. B: Condens. Matter Mater. Phys.*, 1987, **36**(3), 1535–1553, DOI: **10.1103/PhysRevB.36.1535**.

37 W. J. Kendrick, M. Jirásek, M. D. Peeks, G. M. Greetham, I. V. Sazanovich, P. M. Donaldson, M. Towrie, A. W. Parker and H. L. Anderson, Mechanisms of IR amplification in radical cation polarons, *Chem. Sci.*, 2020, **11**(8), 2112–2120, DOI: **10.1039/c9sc05717j**.

38 Y. Guo, B. Zou, F. Yang, X. Zheng, H. Peng and J. Wang, Dielectric polarization effect and transient relaxation in FAPbBr3 films before and after PMMA passivation, *Phys. Chem. Chem. Phys.*, 2021, **23**(17), 10153–10163, DOI: **10.1039/d1cp01136g**.

39 J. Nishida, S. C. Johnson, P. T. S. Chang, D. M. Wharton, S. A. Dönges, O. Khatib and M. B. Raschke, Ultrafast infrared nano-imaging of far-from-equilibrium carrier and vibrational dynamics, *Nat. Commun.*, 2022, **13**(1), 1083, DOI: **10.1038/s41467-022-28224-9**.

40 B. Guzelturk, T. Winkler, T. W. J. van de Goor, M. D. Smith, S. A. Bourelle, S. Feldmann, M. Trigo, S. W. Teitelbaum, H.-G. Steinrück, G. A. La Pena, R. de; Alonso-Mori, D. Zhu, T. Sato, H. I. Karunadasa, M. F. Toney, F. Deschler and A. M. Lindenberg, Visualization of dynamic polaronic strain fields in hybrid lead halide perovskites, *Nat. Mater.*, 2021, **20**(5), 618–623, DOI: **10.1038/s41563-020-00865-5**.